

Experiment Report Form

The double page inside this form is to be filled in by all users or groups of users who have had access to beam time for measurements at the ESRF.

Once completed, the report should be submitted electronically to the User Office via the User Portal:

<https://www.esrf.fr/misapps/SMISWebClient/protected/welcome.do>

Reports supporting requests for additional beam time

Reports can be submitted independently of new proposals – it is necessary simply to indicate the number of the report(s) supporting a new proposal on the proposal form.

The Review Committees reserve the right to reject new proposals from groups who have not reported on the use of beam time allocated previously.

Reports on experiments relating to long term projects

Proposers awarded beam time for a long term project are required to submit an interim report at the end of each year, irrespective of the number of shifts of beam time they have used.

Published papers

All users must give proper credit to ESRF staff members and proper mention to ESRF facilities which were essential for the results described in any ensuing publication. Further, they are obliged to send to the Joint ESRF/ ILL library the complete reference and the abstract of all papers appearing in print, and resulting from the use of the ESRF.

Should you wish to make more general comments on the experiment, please note them on the User Evaluation Form, and send both the Report and the Evaluation Form to the User Office.

Deadlines for submission of Experimental Reports

- 1st March for experiments carried out up until June of the previous year;
- 1st September for experiments carried out up until January of the same year.

Instructions for preparing your Report

- fill in a separate form for each project or series of measurements.
- type your report, in English.
- include the reference number of the proposal to which the report refers.
- make sure that the text, tables and figures fit into the space available.
- if your work is published or is in press, you may prefer to paste in the abstract, and add full reference details. If the abstract is in a language other than English, please include an English translation.



	Experiment title: Multiscale approach for the study of deformation mechanism of new semicrystalline polymers with elastomeric properties	Experiment number: MA-3275
Beamline: BM26B	Date of experiment: from: 3 rd October, 2016 to: 5 th October, 2016	Date of report: 1/3/2017
Shifts: 6	Local contact(s): Daniel Hermida-Merino, (email: hermidam@esrf.fr)	<i>Received at ESRF:</i> 23/05/2017
Names and affiliations of applicants (* indicates experimentalists): Anna Malafronte Rocco Di Girolamo Miriam Scoti		

Report:

In our continued search for polymers having apparently irreconcilable properties such as high level of crystallinity and/or high glass transition temperature coupled with elastomeric properties, such as crystalline block copolymers, our studies have recently focused on isotactic 1,2-poly((*E*)-3-methyl-1,3-pentadiene) (iPE3MPD), a new polymer showing interesting elastomeric properties in spite of a glass transition temperature of 30 °C. iPE3MPD has been recently synthesized with a new class of catalysts,¹ based on cobalt phosphine complexes.

The deformation mechanism at the origing of the elastomeric properties of iPE3MPD is here investigated by time-deformation resolved simultaneous SAXS/WAXS synchrotron measurements. Measurement were performed at Dutch-Belgian beam line BM26-Dubble of ESRF (Grenoble, France). The wavelength of incident X-rays was $\lambda = 0.10402$ nm and the sample to detector distance was 0.27 m for WAXS and 4.58 m for SAXS measurements. The covered range for the scattering vector q was 6–30 nm⁻¹ for WAXS and 0.6-1.8 nm⁻¹ for WAXS data, where q is equal to $q = 4\pi \sin\theta / \lambda$, and 2θ is the scattering angle. Stripes of initial gauge length 15 mm, and width of 5 mm, have been cut from a compression molded film having thickness of 0.41 mm, and mounted in a Linkam tensile stage TST350. Sample jaws move in opposite directions and scattering data have been collected in transmission, using a highly collimated incident beam hitting the sample at the center of the gauge length with a size of 200 μ m \times 200 μ m. Scattering data have been collected at a rate of 1 frame/2 s, while deforming the sample at a rate of 10 mm/min. Two consecutive deformation step cycles have been performed, consisting in stretching the sample up to \approx 150% strain (Path 1), and then releasing the tension up to measure force zero, in the first step, and then stretching again the sample up to \approx 210% strain (Path 2) and then releasing the tension up to measure force zero in the second step. The scattered intensities $I(q)$ have then been subtracted for the empty Linkam cell and processed with the program FIT2D^{2,3} and Bubble³ to extract meridional and equatorial profiles, in angular sectors covering a range of $\pm 30^\circ$ around the horizontal (equator) and vertical (meridian) axis for the SAXS patterns and equatorial sections covering a angular sector of $\pm 20^\circ$ around the horizontal (equator) for the WAXS patterns.

The bi-dimensional SAXS and WAXS patterns recorded in situ during stretching are reported in Figure 1, along with the stress-strain curves (Figure 1K). The sample is first stretched up to \approx 150% deformation (A-F,

A'-F', Path 1 of Figure 1). The corresponding stress strain curve (Path 1 of Figure 1K) shows a well pronounced yielding as a consequence of aging. Then the tension is released up to reach null force. The sample recovers only minimally the initial dimensions, achieving a deformation of $\approx 120\%$ (Figure 1G,G'). Successively, the sample is stretched again from $\approx 120\%$ strain up to $\approx 210\%$ deformation (Figure 1G-J, G'-J', Path 2) and also in this case the tension is gradually released (Figure 1J,J') up to measure a null force. At variance with the Path 1, after 10 minutes at the end of the path 2, the sample recovers almost completely the initial deformation of 120% at the end of path 1, and successive hysteresis cycles after 2 become practically coincident.

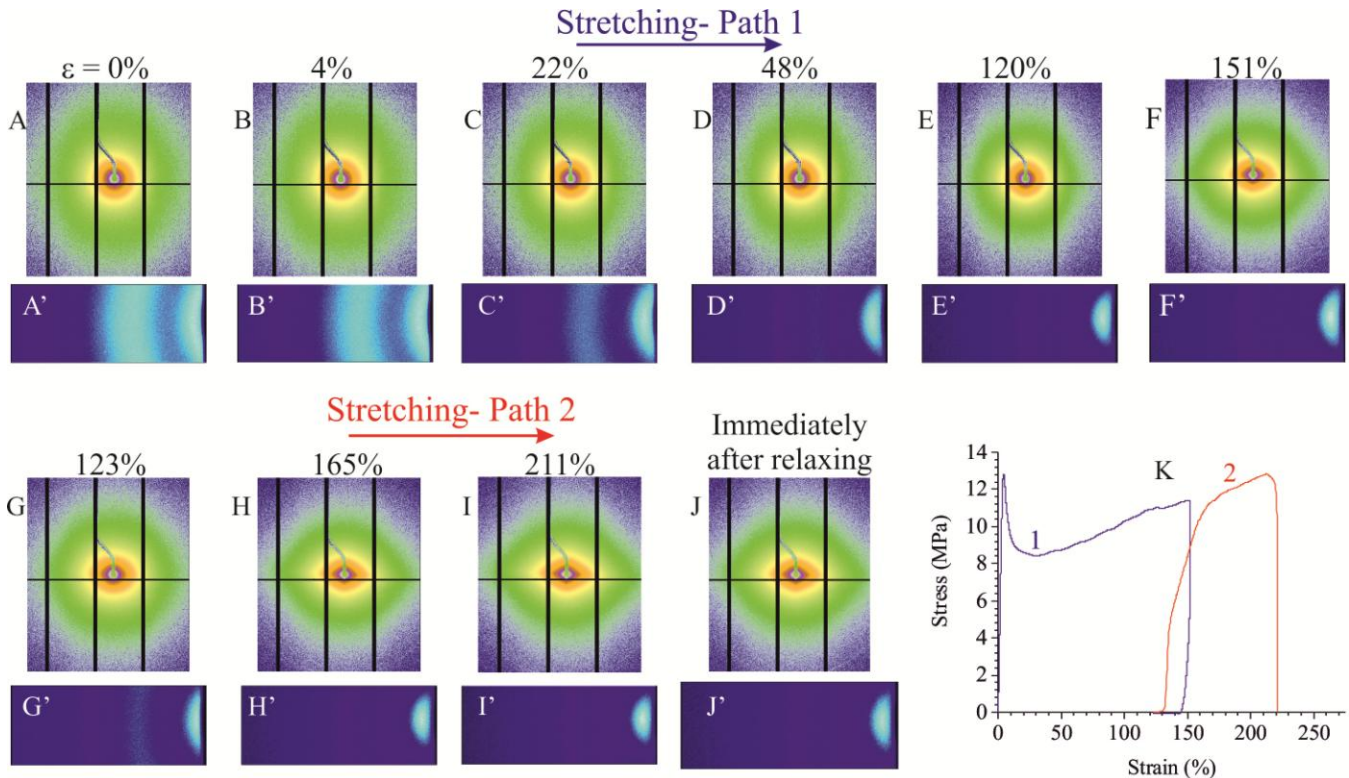


Figure 1. SAXS (A-J) and WAXS (A'-J') collected during two consecutive step cycles of deformation (deformation rate of 10 mm/min) (K) consisting in a first stretching step up to $\approx 150\%$ deformation (A-F, A'-F', Path 1) and successive release of the tension up to measure null force, and in second stretching step from 123% deformation up to $\approx 210\%$ deformation (G-J, G'-J', Path 2).

The WAXS patterns of Figure 1A'-J' reveal in more detail the change in intensity for the two halos on the equator, centered at $q \approx 7$ and 13 nm^{-1} (see also Figure 2). In particular, it is apparent that with increase of deformation, whereas the relative intensity of the first halo increases and tends to become polarized on the equator, the intensity of the second halo tends to decrease (Figure 1A'-F' and G'-J' and Figure 2). Moreover, the halo at $q \approx 13 \text{ nm}^{-1}$ disappears almost completely at the maximum deformation achieved in Path 1 and 2 (Figure 1F', J' and Figure 2A). Upon release of the tension the intensity distribution of the halo at $q \approx 7 \text{ nm}^{-1}$ becomes more isotropic, whereas the relative intensity of the halo at $q \approx 13 \text{ nm}^{-1}$ increases (Figure 1G' and Figure 2A). Ex-situ measurements reveal that, upon stretching, the reflection at $q \approx 13 \text{ nm}^{-1}$ becomes polarized on a well defined layer line, corresponding to a periodicity of $\approx 8 \text{ nm}$ parallel to the stretching direction, and this layer line reflection disappears releasing the tension. This indicates that the crystallization of mesomorphic domains induced by stretching is reversible in consecutive step cycles of deformation and release of the tension.

As shown in Figure 1 A-J, reversible changes occur also at SAXS length scale. In fact, by effect of stretching, the SAXS intensity tends to become polarized on the equator (Figure 1F,I), and upon release of the tension, the intensity distribution becomes more isotropic (Figure 1G). The polarization of intensity achieved at

maximum deformation of $\approx 150\%$ deformation in the Path 1 (Figure 1F), and $\approx 210\%$ deformation in Path 2 (Figure 1I), may be also evidenced by comparing the SAXS profiles on the equator and the meridian, at 0, 151 and 211% deformation in Figure 2B. It is apparent that whereas the equatorial and meridional profiles are coincident for the undeformed sample, at 150 and 211% deformation the intensity on the equator becomes almost one order magnitude higher than the intensity on the meridian. This is the hallmark that, upon stretching, elongated domains with electron density higher than the surrounding matrix are formed, oriented with the long axis in the stretching direction. (Figure 3).

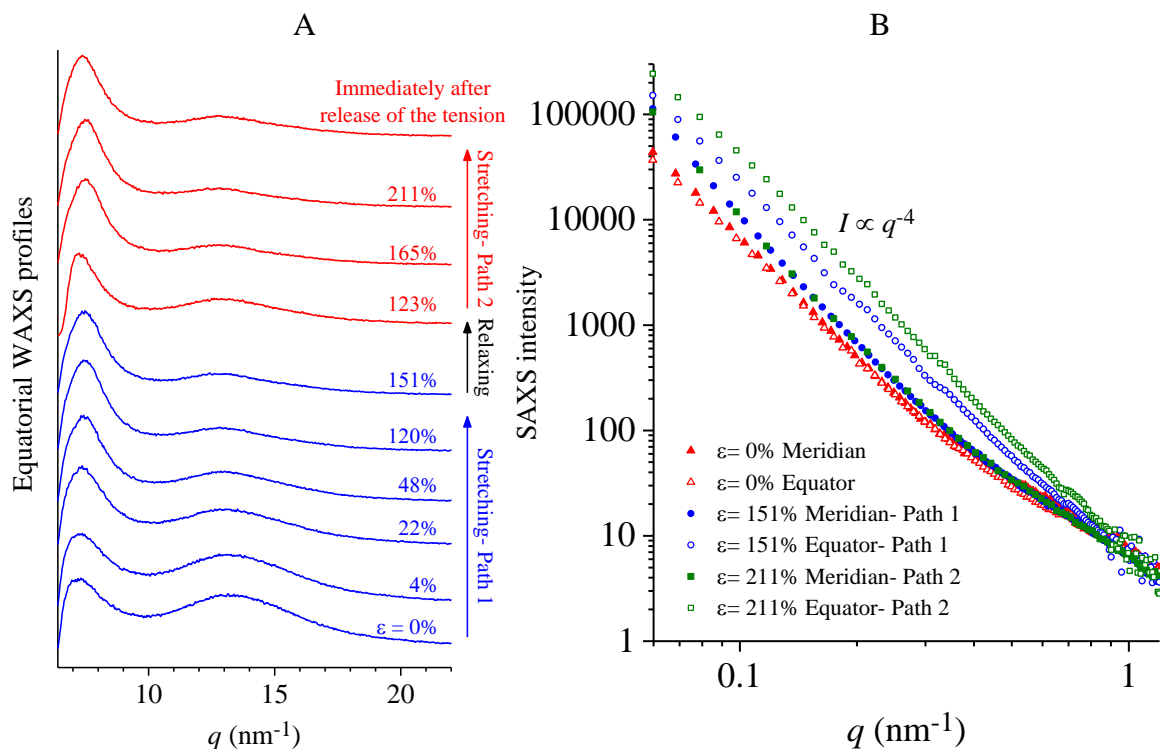


Figure 2. WAXS (A) and SAXS (B) profiles integrated over the equator extracted from the SAXS patterns of Figure 1.

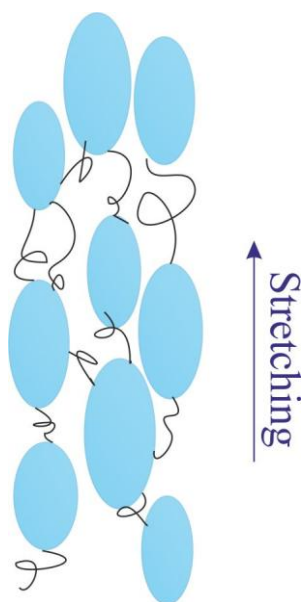


Figure 3. Model of elongated domains of the mesophase, formed by effect of stretching. For simplicity, the domains have been drawn of elliptical shape. They are characterized by no lateral and no longitudinal order.

These preliminary results indicate that the unusual elastomeric properties of iPE3MPD are associated with the stress-induced crystallization of the amorphous phase into a metastable mesophase. Upon release of the tension, the mesomorphic domains “melt” and the sample recovers the initial dimensions. The role of the mesomorphic domains is of providing physical knots of the elastomeric network, preventing the viscous flow of the chains.

References

1. G. Ricci, G. Leone, A. Boglia, F. Bertini, A. C. Boccia, L. Zetta, *Macromolecules* 2009, **42**, 3048.
2. Hammersley, A. P.; Svensson, S.O.; Hanfland, M.; Fitch, A. N.; Häusermann, D. Two-Dimensional Detector Software: From Real Detector to Idealised Image or Two-Theta Scan. *High Pressure Research*. **1996**, *14*, 235-248.
3. Hammersley, A.P.; Svensson, S. O.; Thompson, A. Calibration and correction of spatial distortions in 2D detector systems. *Nucl. Instr. Meth.*, **1994**, *A346*, 312-321.